Probability distributions of landslide tsunamis

Philip Watts[1] and Jose C. Borrero[2]

[1]*Applied Fluids Engineering, Inc., Long Beach, California, U.S.A.*
[2]*Department of Civil Engineering, University of Southern California, Los Angeles, California, U.S.A.*

Abstract. A review of tsunamis during the 1990s reveals 30% of maximum run-up peaks probably involved tsunamigenic mass failure. Submarine mass failure includes underwater slides, underwater slumps, and reef failure, most often triggered by a nearby earthquake. Earthquakes above magnitude 7 are typically accompanied by thousands of mass failure events, although most of these will not be tsunamigenic. A geological context derived from marine surveys is needed to identify prospective mass failures and to predict their size and location. Probabilistic calculations of underwater slides and slumps off of Southern California yield preliminary distributions of mass failure dimensions. Tsunami amplitude is estimated from accurate curve fits based on numerical simulations of mass failure events. As observed, about 36% of all earthquakes generate landslide tsunamis that surpass coseismic displacement. A finite probability exists for mass failure to generate tsunamis with amplitudes in excess of 10 m. The probabilities of nearshore and offshore earthquakes can be converted directly into tsunami hazards from submarine mass failure. Indicators of prospective tsunamigenic landslides such as sedimentation rate or liquid limit improve our ability to predict future events and to assess their impact on coastal populations and development.

1. Introduction

Increased human coastal population and development coupled with devastating losses in recent history motivate tsunami hazard assessment efforts. Tsunamis may be generated by volcanic eruptions, coseismic sea floor displacement, gas hydrate phase change, underwater landslides, and oceanic meteor strikes. Landslide tsunamis remain one of the least studied of these five mechanisms, in part because their occurrence is concealed and in part because of the complicated dynamics involved in failure, center of mass motion, and landslide deformation. Scientists are currently unable to assess some underwater landslide hazards, to predict their occurrence following a nearby earthquake, and to evaluate their tsunamigenic potential. In this paper, we will demonstrate a technique that predicts a frequency and probability distribution of tsunamigenic mass failures off of Southern California.

1.1 Review of recent tsunamis

Historical records verify the tsunami hazards posed by submarine mass failure. Most damage and fatalities during or following the 1964 Good Friday Alaskan earthquake resulted from local waves generated by submarine mass failure (Plafker *et al.*, 1969). Since 1992, there have been at least twelve major local tsunamis. The majority of these tsunamis demonstrated regions of

---

peaked longshore run-up distribution. For example, run-up produced by the Flores Island tsunami showed a modest run-up plateau of 8 m punctuated by numerous large peaks up to 26 m in amplitude that correlated with reef failures and subaerial landslides (Imamura and Gica, 1996). The 1998 Papua New Guinea tsunami has been the subject of extensive marine surveys to describe the slump source and to model the tsunami generation, propagation, and run-up (Tappin *et al.*, 1999, 2001). Five other events, Nicaragua, Mindoro, Skagway, Kamchatka, and Izmit Bay are known or suspected to have involved significant landslide tsunami generation, with or without significant coseismic displacement. Throughout the Pacific, tsunami amplitude and earthquake magnitude records acquired during the 1990s suggest that tsunamigenic submarine mass failures generate the maximum run-up in around 30% of tsunami events.

2.   Types of Submarine Mass Failure

Damaging tsunamis may result from the failure of sediment along steep fjord banks, near boundaries of submarine canyon systems, at active river deltas, along volcanic islands or ridges, or at submerged alluvial plains including continental margins (Hampton *et al.*, 1996). Underwater landslides or mass failures include slides and slumps as two distinct end members of a continuous spectrum of submarine mass failure (Prior and Coleman, 1979; Edgers and Karlsrud, 1982; Schwab *et al.*, 1993). Underwater slides are identified by translational failure, while underwater slumps are defined to undergo rotational failure (Schwab *et al.*, 1993). Terzaghi (1956) showed that underwater slides and slumps can often be related to excess pore water pressures along (at least) the initial failure plane. Prior and Coleman (1979) attribute excess pore water pressure to low tides, artesian water flows, recent external loads, rapid sedimentation, seismic ground motions, construction induced vibrations, volcanic activity, vaporization of gas hydrates, wave action, or any combination of these or similar factors. Most tsunamigenic underwater slides and slumps are triggered by local earthquakes.

2.1   Center of mass motions

Water wave amplitudes above an underwater slide or slump scale with characteristics of center of mass motion (Watts, 1998, 2000). We contrast the center of mass motions of submarine slides and slumps by the dominant retardive force, providing convenient asymptotic limits for these two types of motion. Many real failure events are expected to move in a manner combining aspects of each analysis. As such, these results provide end members for landslide center of mass motions. Center of mass motion is parametrized by the characteristic time of motion t_o and the characteristic distance of motion s_o, where the landslide initial acceleration $a_o = s_o/t_o{}^2$ governs tsunami generation. These quantities are ultimately dependent on the sediment type and density as well as the landslide shape (Watts, 1998).

2.1.1 Underwater slides

Dobry *et al.* (1982) and Seed *et al.* (1988) show that sand and silt can experience an order of magnitude drop in shear strength during failure, thereby justifying neglect of Coulomb friction in center of mass motion. The frictionless motion of a noncohesional slide is limited primarily by fluid dynamic drag. The solution of the equation of motion becomes

$$s(t) = s_o \ln \left[\cosh(\frac{t}{t_o}) \right] \tag{1}$$

which provides the slide center of mass position along a straight incline as a function of time subject to the initial condition $s(0) = 0$. Underwater slide motion is characterized by specific density γ, length along the incline b, and incline angle θ. These quantities can be estimated from bathymetry data acquired during a marine survey of suspected tsunami sources.

2.1.2 Underwater slumps

We model a slump as a rigid body moving along a circular arc subject to external moments from added mass, buoyancy, gravity, and shear stress along the failure plane. The rotation of a cohesive slump is retarded by significant basal friction that can keep fluid dynamic drag from reaching important scales. The critical state shear stress along the failure plane is assumed to remain constant during motion (Bardet, 1997). Multiplying the angular position by the radius of curvature gives the slump center of mass position along the failure arc

$$s(t) = s_o \left[1 - \cos(\frac{t}{t_o}) \right] \tag{2}$$

where $s(0) = 0$ and (2) remains valid for times $0 < t/t_o < \pi$. Underwater slumps require a radius of curvature R and the angular rotation $\Delta\phi$ to describe motion. These quantities require more sophisticated seismic reflection marine surveys.

3. Landslide Tsunami Generation

In this work, we employ the model problem whereby an underwater slide or slump is modeled as a semi-ellipse resting on a straight incline with angle θ from horizontal (Grilli and Watts, 1999). The semi-ellipses have a maximum thickness T along half of the minor axis that is perpendicular to a major axis of total length b (Grilli and Watts, 1999). The semi-ellipse has an initial vertical submergence d at the middle. We prescribe the slide or slump center of mass motion along the incline by either (1) or (2) and assume negligible deformation. Our results apply specifically to two-dimensional geometries, a criterion that may be met by less than half of all tsunamigenic mass failures. Numerical experiments have been reduced to predictive curve fits of tsunami amplitude that are simple analytical functions of nondimensional quantities (Watts *et al.*, 2001). The maximum tsunami amplitude above the initial

mass failure location is chosen here as a characteristic tsunami amplitude (Watts, 1998, 2000). We consider the semi-ellipse as a good approximation of most underwater slide and slump shapes, whereas the solutions for center of mass motion represent two end members between which there are many possible variations. Nevertheless, the curve fits provide a rapid and inexpensive means to estimate tsunami amplitude and gauge the sensitivity of that amplitude on landslide characteristics.

3.1 Underwater slides

Tsunamis generated by slides are somewhat simpler to describe than slumps because their decelerational motion occurs in deeper water, often after tsunami generation and propagation. A two-dimensional tsunami amplitude equation was formulated for thin, linear slides that experience negligible basal friction but significant fluid dynamic drag

$$\eta_{2d} \approx s_o \left(0.0506 \sin^{1.18}\theta - 0.0328 \sin^{2.18}\theta\right) \left(\frac{T}{b}\right) \left(\frac{b}{d}\right)^{1.25} \tag{3}$$

where s_o is contained in (1). Equation (3) has an intrinsic amplitude accuracy of $\pm 6\%$ if the slide shape and motion are exact. The constraints to (3) are that $\theta < 30°$, $T/b < 0.2$, and $d/b > 0.06$.

3.2 Underwater slumps

Slumps often travel only a fraction of their length and therefore come to rest near their initial position. A two-dimensional tsunami amplitude equation was formulated for deep-seated, rotational slumps that experience strong basal friction but minimal fluid dynamic drag

$$\eta_{2d} \approx s_o \Delta\phi^{1.39} \left(0.80\sin\theta - 2.48\sin^2\theta + 2.54\sin^3\theta\right) \left(\frac{T}{b}\right) \left(\frac{b}{d}\right)^{1.25} \left(\frac{b}{R}\right)^{0.63} \tag{4}$$

where s_o is contained in (2). Equation (4) has an intrinsic amplitude accuracy of $\pm 3\%$ if the slump shape and motion are exact. The constraints to (4) are that $\theta < 30°$, $\Delta\phi < 0.53$, $T/b < 0.2$, $1 < R/b < 2$, and $d/b > 0.06$.

4. Probabilistic Model Description

A predictive model is developed to examine the probability distribution of tsunami amplitudes generated by submarine mass failure. The model uses realistic uniform or Poisson probability distributions to span the complete parameter space of nearshore geology off of Southern California. Each model parameter is treated randomly in what is effectively a Monte-Carlo scheme. Here, the term "random" refers to a quasi-random number between zero and one that has been seeded with the starting date of the simulations expressed as an integer. The dependence and sensitivity of tsunami amplitude with

respect to each random parameter is readily evaluated. The model is divided into three sections: earthquake engineering characteristics, sediment stability calculations, and tsunami amplitude estimates. We ask the question: what parameters along the presumed failure plane govern or dominate tsunamigenic landslides?

4.1   Earthquake engineering characteristics

Seismic hazards in Southern California have been summarized by the Working Group on California Earthquake Probabilities (1995). Our model begins by choosing a random earthquake magnitude

$$\mathrm{M_w} = 3\ \mathrm{random}\ + 4.4 \tag{5}$$

that uniformly covers the $4.4 < \mathrm{M_w} < 7.4$ magnitude range expected to cause landslides off of Southern California. The distance of the earthquake epicenter from the continental slope is chosen at random from within a reasonable range of influence that depends on moment magnitude

$$x = 2\ \mathrm{random}\ 10^{\mathrm{M_w}-5} \tag{6}$$

where x is expressed in units of kilometers (Kramer, 1996). Outside of this range of influence, ground shaking does not usually cause mass failure on land. Kramer (1996) provides a curve fit for peak horizontal acceleration with respect to earthquake moment magnitude assuming a nominal hypocenter depth of $h = 5.57$ km

$$a_{\mathrm{pha}} = g10^{-0.105+0.229(\mathrm{M_w}-6)-0.778\log(r)+0.251} \tag{7}$$

where r is the radial distance in kilometers from the hypocenter to the continental slope, and the logarithm is taken with respect to base 10.

4.2   Sediment stability calculations

Schwab *et al.* (1993) describe the geological context of the Southern California margin as well as several significant mass failure events. This and other studies provide sediment characteristics and sedimentation rates needed to model sediment response to a nearby earthquake. We did not consider the effects of sediment inhomogeneities, seismic and landslide histories, overconsolidation, addition of a recent overburden, liquefaction, or storm waves in our calculations. The sediment stability is assessed along a continental slope obtained from the cumulative Poisson distribution

$$\theta = -6.4\ln{(\mathrm{random})} \tag{8}$$

where the mean slope is $6.4°$ and (8) is truncated at a maximum slope of $25°$. We assume a bulk sediment density of 1900 kg/m^3 throughout this work.

   The main effort in our stability calculations consists of estimating pore water pressure at the presumed failure plane. This requires, among other factors, simulating pore pressure diffusion during sediment consolidation

(Terzaghi, 1956). Our model randomly chooses a mean sedimentation rate for the continental slope. The mean sedimentation rate W is chosen from a cumulative Poisson distribution

$$W = -0.003 \ln (\text{random}) \qquad (9)$$

with an expected rate of 3 mm/year. Historical sedimentology of the Santa Monica Basin is described by Schwalbach *et al.* (1996) and Gorsline (1996). A nominal pore pressure u is prescribed to account for coastal uplift or subsidence, artesian water flows, tidal fluctuations, and other related effects that may be present at the time of the earthquake. The nominal pore pressure

$$u = -50 + 100(\text{random}) \qquad (10)$$

can reach a maximum of ± 50 Pa. Sediment is built up based on a randomly calculated yearly sediment load followed by pore water diffusion for the rest of that year. The mean sediment load is prescribed by W whereas the actual sediment load in any given year is assumed to be determined by a random Poisson distributed flood event. The accumulation of yearly sediment enables pore water pressure to build and contribute to failure. During any given year, the pore water pressure is reduced by diffusion according to

$$U_w = U_o \operatorname{Erf} \left(\frac{0.5T}{\sqrt{3.1536 \times 10^7 c_v}} \right) \qquad (11)$$

where U_o is the pore water pressure of the previous year plus the nominal pore pressure u plus the random sedimentary overburden of that year (Bardet, 1997). The parameter T is the current depth of the failure plane, and c_v is the pore water diffusion coefficient. We assume that a sufficiently thick sediment blanket exists to accommodate failure up to a maximum thickness of $T = 800$ m.

Earthquake and sediment parameters become inputs in the sediment failure calculation (Morgenstern and Price, 1965). We employ an infinite slope, quasi-static stability analysis because of its moderate accuracy and its relative simplicity (Turner and Schuster, 1996). The randomness in (11) introduced through U_o precludes a direct computation of the failure depth. Failure occurs when the unstable depth becomes less than or equal to the current depth T of sediment accumulated from the start of the simulation. It is as if the earthquake triggering the landslide were happening every year, although this appearance is merely an artifact of the sensitivity analysis. Instead, some random parameters along the failure plane remain fixed while other random parameters depend on the consolidation history of the sediment. The yearly sedimentation loads and stability analyses are a means of testing the relative importance of fixed parameters *versus* consolidation dependent parameters. The goal is to discover which random parameters at the failure plane, if any, control or dominate failure. We associate slides with sandy/silty sediment along the failure plane; whereas we associate slumps with clayey sediment along the failure plane. Two different shear strength and water diffusion models are introduced for the two kinds of sediment considered here, respectively. Schwab *et al.* (1993) estimate that nearly half of all mass failures off of the continental United States appear to satisfy translational sliding, while the other half appear to satisfy rotational slumping.

4.2.1 Underwater slides

Slides are often associated with sandy or silty sediments, perhaps deposited in thin bedded layers that serve as failure planes. The model chooses a random friction angle ϕ in degrees, cohesion c in Pascals, and pore water diffusion coefficient c_v in m^2/s that are suitable for sands and silts.

$$\phi = 25 + 10 \text{ random} \tag{12}$$

$$c = 100,000 \text{ random} \tag{13}$$

$$c_v = 10^{-6} + 10^{-5} \text{ random} \tag{14}$$

The range in parameter values is meant to reflect variations in clay content and size distribution of the sediment grains.

4.2.2 Underwater slumps

Slumps are often associated with clayey sediments that fail by rotation along rounded arcs. The model chooses random plasticity indices PLI and liquid limits LL as fundamental and independent descriptors of the clay physical properties. These two parameters provide shear strength and pore water diffusivity from standard curve fits (Bardet, 1997).

$$PLI = 100 \text{ random} \tag{15}$$

$$LL = \text{ random} \tag{16}$$

$$S_u = (0.11 + 0.0037 \ PLI)(10^{-2LL})\frac{4}{9}T(\rho_b - \rho_o)g\cos\theta \tag{17}$$

$$c_v = 10^{-8} + \frac{10^{-6}}{1 + PLI} \tag{18}$$

where the term farthest on the right hand side of (17) is an approximation of the mean normal stress exerted by the slump mass.

4.3 Tsunami amplitude estimates

The depth d in meters at the middle of a potential mass failure is chosen by

$$d = 500 + 1000 \text{ random} \tag{19}$$

assuming a failure that spans a significant fraction of the continental slope. The model randomly chooses the mass failure length according to the sediment type. Underwater slides often exhibit maximum thickness to initial

length ratios of $T/b = 1\text{--}4\%$ (Prior and Coleman, 1979; Turner and Schuster, 1996)

$$b = (25 + 75 \text{ random})T \tag{20}$$

$$s_o \approx 4.4825 \, b \tag{21}$$

where the characteristic distance of motion s_o follows from the analyses of Watts *et al.* (2001). Underwater slumps often involve deep failure with maximum thickness to initial length ratios of $T/b = 7\text{--}20\%$ (Prior and Coleman, 1979; Turner and Schuster, 1996)

$$b = (5 + 10 \text{ random})T \tag{22}$$

$$R \approx \frac{b^2}{8T} + \frac{T}{2} \tag{23}$$

$$s_o \approx \frac{9S_u R}{4Tg(\rho_b - \rho_o)} \tag{24}$$

where the radius of curvature R and the characteristic distance of motion s_o follow from the analyses of Watts *et al.* (2001).

4.4   Limitations and constraints

Our analyses of slope stability assume an infinite slope as well as yearly deposition of a uniform sediment. These approximations arise because we assume complete knowledge of the sediment along the failure plane without attempting to track the long-term evolution of the continental slope itself. Because we study a single failure per earthquake, our results apply to the worst case failure or largest possible landslide tsunami. Likewise, the two-dimensional tsunami amplitude calculated here is an upper bound on the tsunami amplitude generated by a landslide with finite width. We have attempted to use uniform probability distributions whenever possible. On the one hand, some combinations of sediment parameters may not be realizable in practice, although this is a subject of further research through boring of continental margins. On the other hand, some parameter ranges could be extended to account for physically plausible extreme events, such as large spikes in transient water pressure along existing faults. The next step in this work would be to evaluate the role of probability distribution shapes on landslide occurrence and tsunami amplitudes.

5.   Probabilistic Model Results

The results given here are general and subject to revision should a specific site be chosen for careful study. The two-dimensional tsunami amplitude given here occurs above the underwater slide or slump and is a simplistic

measure of tsunami hazard. Three-dimensional effects could significantly reduce tsunami amplitudes. Figure 1 refutes two commonly held assumptions regarding landslide tsunamis. First of all, large tsunamis can be generated with roughly equal probability by earthquakes with moment magnitudes ranging from 4.5–7. This result is not substantially modified if one considers peak horizontal acceleration as the independent parameter. Landslide tsunami amplitude is largely independent of earthquake magnitude. The same is true for the continental slope angle. Almost all of the structure seen in Fig. 1b is either random, or a direct consequence of the Poisson probability distribution, with the sole exception of very small incline angles. We conclude that slope is not a significant predictor of tsunamigenic landsliding. Almost all of the random parameters produced plots similar to these for both slides and slumps.

Figure 2 relates two-dimensional tsunami amplitude to the mean sedimentation rate, which is the only random parameter with any significant correlation for slides. Because Fig. 2a resembles Fig. 1b, we surmise that the large tsunami amplitudes at large sedimentation rates may be the origin of the correlation. Maximum slide thickness is not an independent parameter in our work, but it is nevertheless a good predictor of tsunami amplitude. A similar plot may be made for slide length given that length and thickness are proportional. Figure 3 shows that tsunamigenic slumps occur primarily in regions of low liquid limit LL or high sediment strength (Bardet, 1997). Cores taken off of Papua New Guinea in the source region of the 1998 tsunami revealed stiff clay (Tappin *et al.*, 2001). For slumps, we also find that failure thickness is an important predictor of tsunami amplitude. We speculate that mass failure is more probable in sediments with low strength, although failure tends to be thin and not particularly tsunamigenic.

5.1 Frequency of landslide tsunamis

We find that earthquakes fail to generate any failure in clayey sediments 20% of the time and in sandy/silty sediments 50% of the time, neglecting liquefaction as a failure mechanism. Landslide tsunamis greater than 1 cm should be generated by approximately 47% of all earthquakes. In agreement with observations, we find that 36% of landslide tsunamis surpass an estimate of the vertical coseismic displacement of the earthquake that triggered failure. The Working Group on California Earthquake Probabilities (1995) places the probability of significant offshore earthquakes at 0.06–0.07 per year. The recurrence interval off of Southern California is therefore once every 15 years over the entire range of earthquake magnitudes considered here. We find that a landslide tsunami with an amplitude greater than 1 m can be expected off of Southern California about every 75 years. Historical records indicate two such events in the last two centuries, the 1812 Santa Barbara tsunami and the 1927 Point Arguello tsunami (McCulloch, 1985).
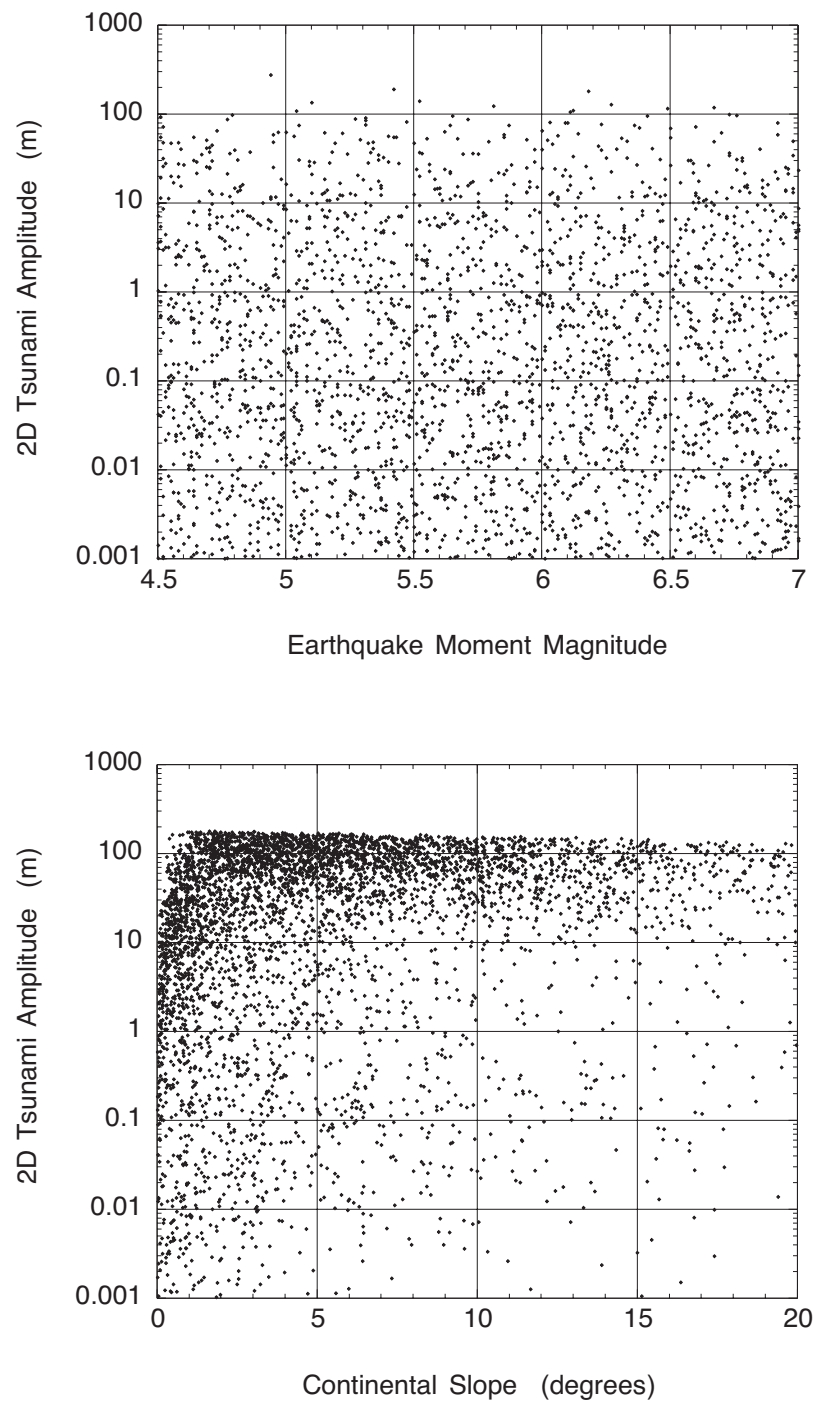
Figure 1: Two quantities that do not correlate with landslide tsunami amplitude.
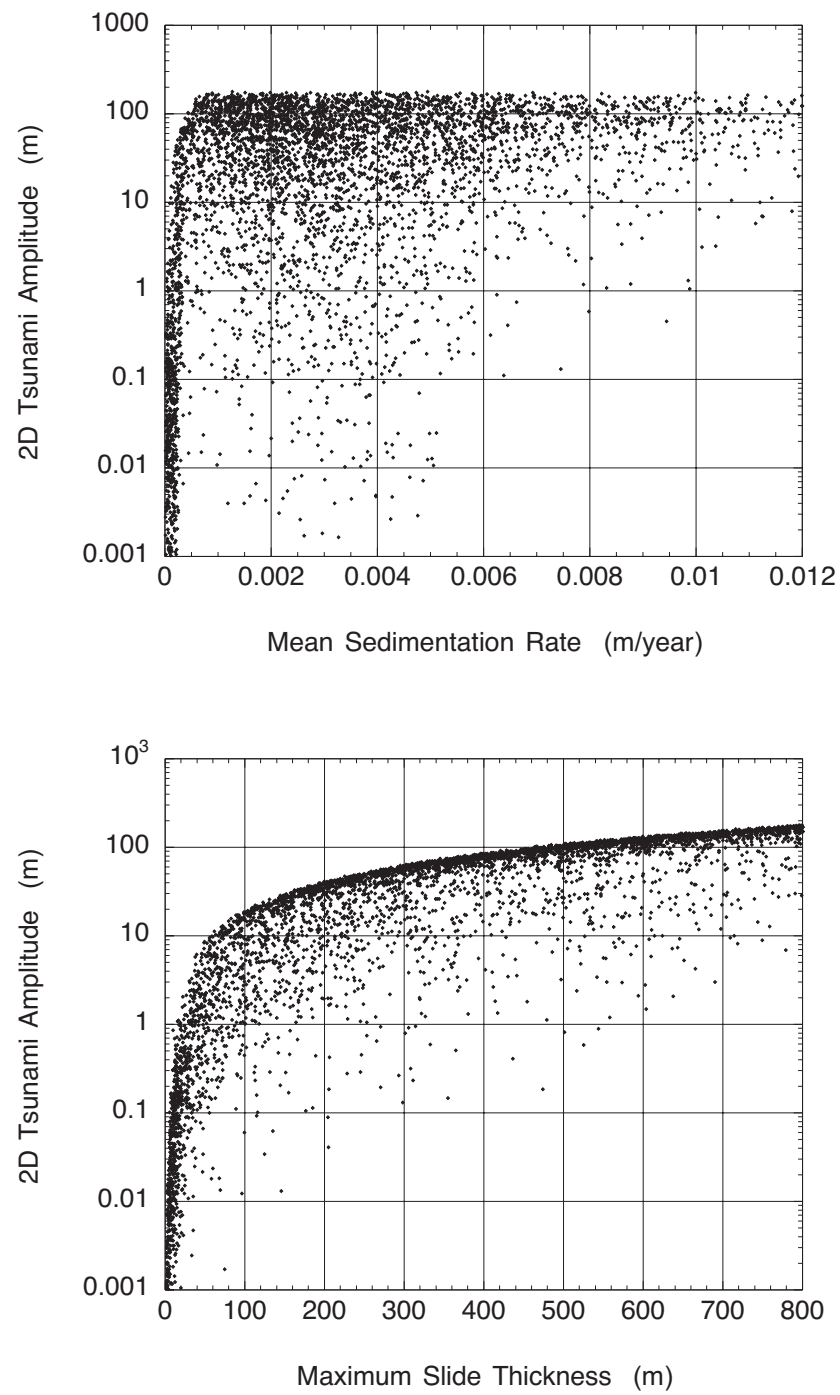
Figure 2: Two quantities that describe underwater slide tsunami amplitude.
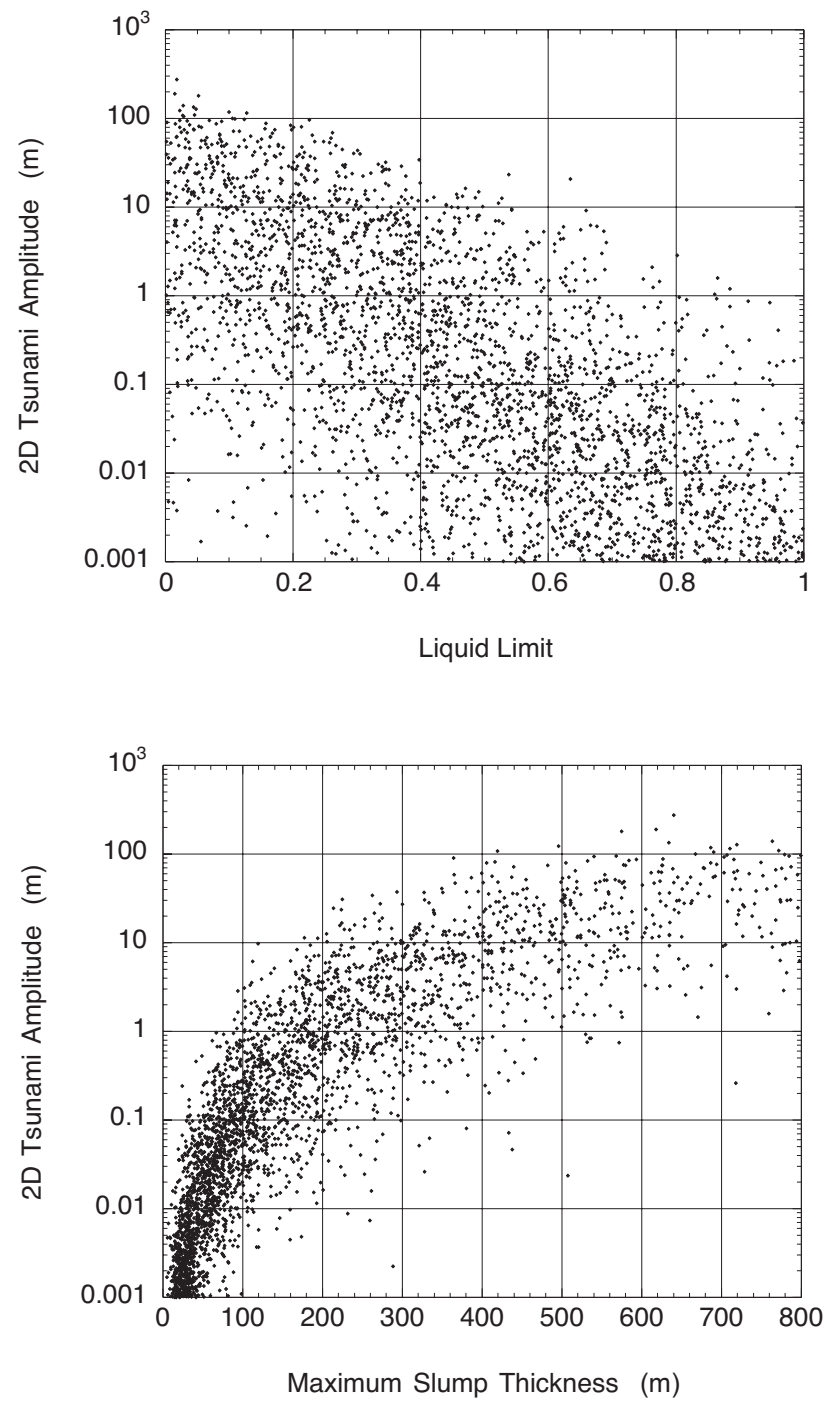
Figure 3: Two quantities that describe underwater slump tsunami amplitude.

6.   Conclusions

We present an estimate of tsunami hazards from submarine mass failure for Southern California. The two-dimensional tsunami amplitude curve fits used herein enable rapid case studies and tsunami hazard assessment. In particular, we show that peaks in tsunami amplitude such as the 26 m wave that devastated Riangkroko, Indonesia in 1992 could have been expected from local tsunamigenic landslides. Off of Southern California, the potential exists to generate local tsunami amplitudes in excess of 10 m, although further study is needed to identify specific sites and to assess the probabilities of any such events. To that end, a handful of parameters have been shown to significantly influence tsunamigenic landsliding: mean sedimentation rate W for sandy or silty slopes, liquid limit LL for clayey slopes, and the resulting maximum thickness of failure T for any sediment type. Other parameters studied here may strongly influence the morphology and evolution of a margin even if they do not correlate with tsunami amplitude. The ensemble of landslide tsunamis produced in this study seems to capture some general features of the ensemble of landslide tsunamis observed throughout the Pacific during the 1990s. The tsunami probabilities calculated here also appear to fit historical tsunamigenicity off of Southern California. Despite these promising results, we cannot claim that we have reproduced the correct probability distribution for landslide tsunamis because a greater variety of constitutive relations, failure mechanisms, and probability distributions need to be considered for the sake of completeness. For any site specific study, the parameter ranges would need to be significantly reduced.

7.   References

Bardet, J.-P. (1997): *Experimental soil mechanics*. Prentice Hall, Upper Saddle River, New Jersey.

Dobry, R., R.S. Ladd, F.Y. Yokel, R.M. Chung, and D. Powell (1982): *Prediction of pore water pressure buildup and liquefaction of sands during earthquakes by the cyclic strain method*. NBS Building Science Series 138, Nat. Bureau Standards, U.S. Dept. of Commerce, Washington, D.C.

Edgers, L., and K. Karlsrud (1982): Soil flows generated by submarine slides: Case studies and consequences. *Nor. Geotech. Inst. Bull., 143,* 1–11.

Gorsline, D.S. (1996): Depositional events in Santa Monica Basin, California Borderland, over the past five centuries. *Sed. Geol., 104,* 73–88.

Grilli, S.T., and P. Watts (1999): Modeling of waves generated by a moving submerged body: Applications to underwater landslides. *Eng. Anal. Boundary Elements, 23*(8), 645–656.

Hampton, M. A., H.J. Lee, and J. Locat (1996): Submarine landslides. *Rev. Geophys., 34*(1), 33–59.

Imamura, F., and E.C. Gica (1996): Numerical model for tsunami generation due to subaqueous landslide along a coast. *Sci. Tsunami Hazards, 14,* 13–28.

Kramer, S.L. (1996): *Geotechnical Earthquake Engineering.* Prentice Hall, Upper Saddle River, New Jersey.

McCulloch, D.S. (1985): *Evaluating earthquake hazards in the Los Angeles region— An earth science perspective.* In Prof. Paper 1360, U.S. Geol. Survey, U.S. Dept. of Interior, Menlo Park, CA.

Morgenstern, N.R., and V.E. Price (1965): The analysis of the stability of general slip surfaces. *Geotechnique, 15,* 79–93.

Plafker, G., R. Kachadoorian, E.B. Eckel, and L. Mayo (1969): The Alaska earthquake March 27, 1964: Various communities. U.S. Geol. Surv. Prof. Paper 542-G, U.S. Dept. of Interior, Washington, D.C.

Prior, D.B., and J.M. Coleman (1979): Submarine landslides: Geometry and nomenclature. *Z. Geomorph. N. F.*, *23*(4), 415–426.

Schwab, W.C., H.J. Lee, and D.C. Twichell (1993): Submarine landslides: Selected studies in the U.S. exclusive economic zone. U.S. Geol. Surv. Bull. 2002, U.S. Dept. of Interior, Washington, D.C.

Schwalbach, J.R., B.D. Edwards, and D.S. Gorsline (1996): Contemporary channel-levee systems in active borderland basin plains, California Continental borderland. *Sed. Geol., 104,* 53–72.

Seed, H.B., R.B. Seed, F. Schlosser, F. Blondeau, and I. Juran (1988): The landslide at the Port of Nice on October 16, 1979. *Rep. No. UCB/EERC-88/10,* Earthquake Engineering Research Center, University of California, Berkeley, California.

Tappin, D.R., T. Matsumoto, and shipboard scientists (1999): Offshore geological investigation of the July 1998 Sissano tsunami, Papua New Guinea. *Eos Trans. AGU, 80*(30), 329.

Tappin, D.R., P. Watts, G.M. McMurtry, Y. Lafoy, and T. Matsumoto (2001): The Sissano, Papua New Guinea tsunami of July 1998—Offshore Evidence on the source mechanism. *Mar. Geol., 175,* 1–23.

Terzaghi, K. (1956): Varieties of submarine slope failures. *Proc. 8th Texas Conf. Soil Mech. Found. Eng.,* 1–41.

Turner, A.K., and R.L. Schuster (1996): *Landslides: Investigation and mitigation.* Special Report 247, Trans. Res. Board, National Academy Press, Washington, D.C.

Watts, P. (1998): Wavemaker curves for tsunamis generated by underwater landslides. *J. Waterway Port Coast. Ocean Eng., ASCE, 124*(3), 127–137.

Watts, P. (2000): Tsunami features of solid block underwater landslides. *J. Waterway Port Coast. Ocean Eng., ASCE, 126*(3), 144–152.

Watts, P., S.T. Grilli, and C.E. Synolakis (2001): Tsunami generation by submarine mass failure. I: Wavemaker models. *J. Waterway Port Coast. Ocean Eng., ASCE,* submitted.

Working Group on California Earthquake Probabilities (1995): Seismic hazards in Southern California: Probable earthquakes, 1994 to 2024. *Bull. Seismol. Soc. Am., 85*(2), 379–439.